Effect of crowding and confinement on first-passage times: A model study

C. Antoine* and J. Talbot†

Laboratoire de Physique Théorique de la Matière Condensée, UPMC, CNRS UMR 7600, Sorbonne Universités, 4 place Jussieu, 75252 Paris Cedex 05, France

(Received 23 March 2016; revised manuscript received 23 May 2016; published 14 June 2016)

We study the "color dynamics" of a hard-disk fluid confined in an annulus, as well as the corresponding hard-sphere system in three dimensions, using event-driven simulation in order to explore the effect of confinement and self-crowding on the search for targets. We compute the mean first-passage times (MFPTs) of red particles transiting from the outer to the inner boundary as well as those of blue particles passing from the inner to the outer boundary for different packing fractions and geometries. In the steady state the reaction rate, defined as the rate of collision of red particles with the inner boundary, is inversely proportional to the sum of the MFPTs. The reaction rate is wall mediated (ballistic) at low densities and diffusion controlled at higher densities and displays a maximum at intermediate densities. At moderate to high densities, the presence of layering has a strong influence on the search process. The numerical results for the reaction rate and MFPTs are compared with a ballistic model at low densities and a Smoluchowski approach with uniform diffusivities at higher densities. We discuss the reasons for the limited validity of the theoretical approaches. The maximum in the reaction rate is qualitatively well rendered by a Bosanquet-like approach that interpolates between the two regimes. Finally, we compute the position-dependent diffusivity from the MFPTs and observe that it is out of phase with the radial density.

DOI: 10.1103/PhysRevE.93.062120

I. INTRODUCTION

How does crowding affect the encounter rate of a particle with a target? The answer to this question has great significance, particularly in biophysics [1–6], but also in other fields [7] such as ecology [8], finance, and computer science. An important example is the cell cytoplasm, where crowding agents typically occupy 20%–30% of the total volume and strongly influence the kinetics and thermodynamics of cellular reactions [9,10].

Smoluchowski theory provides a simple expression for the rate of reaction between a diffusing particle and a sink but is strictly valid only in the infinite dilution limit. Dzubiella and McCammmon [11] developed a modified Smoluchowski approach to describe systems with a low density of diffusing particles and Kim and Yethiraj [12] incorporated structural information to obtain quantitative agreement with molecular dynamics simulations of an association reaction in a hard-sphere fluid. Dorsaz *et al.* [13,14] extended this approach in a study of the encounter rate of hard spheres with an immobilized target (particles that touch the sink are absorbed and repositioned to an outer buffer zone). By taking into account density oscillations, they obtained good agreement with event-driven Brownian dynamics simulations.

Confinement, in addition to crowding, is frequently present in biological systems. For example, the cytoskeleton divides the cell into compartments [9]. Schmit *et al.* [15] included both effects in a lattice model consisting of one reacting particle and a fixed number of inert particles contained in a circular domain. The reaction rate is low in both large and small systems, where concentration and crowding, respectively, are limiting, and is maximized at an intermediate confinement when 50% of the lattice sites are occupied.

The structure of confined fluids may be strongly modified compared with that of bulk systems [16–20]. For example, a slit pore induces a spatially inhomogeneous density profile, or "layering," in a hard-sphere fluid, resulting in a position-dependent diffusion coefficient [21]. This suggests that one should not rely on lattice models [15], which cannot display layering, to provide accurate descriptions at moderate to high densities.

When a diffusing particle reacts instantaneously with a sink the reaction rate is simply the inverse of the mean first-passage time (MFPT). First-passage processes of diffusive trajectories in a homogeneous environment are well understood [22] and there are also a few studies in complex geometries [23] and for swarms of independent searchers [24]. The majority of published work addressing first-passage-time problems considers model systems with a constant, uniform diffusivity. In many applications, however, the diffusivity is not uniform. The cellular content is obviously heterogeneous, as are larger scale biological systems. For example, tumors generally consist of distinct layers whose diffusion coefficients can differ by factors of 3–4 and habitats in ecological applications are typically heterogeneous [25,26].

First-passage processes may also involve ballistic trajectories [22,27,28]. In the transport of dilute gases through mesoporous materials, the usual diffusion process may be replaced by the so-called "Knudsen regime," where molecule-wall, rather than gas-gas, collisions are dominant. Assuming that the molecule-wall collisions are uncorrelated, the Knudsen theory [29–33] implies that the direction of a rebounding molecule is distributed according to a cosine law. As explained below, this may help in modifying the usual diffusive MFPT formulas to account for the ballistic trajectories for either a low density or a strong confinement.

In this study we examine a model two-dimensional (2D) system consisting of N hard disks confined in an annulus, as well as the corresponding 3D system of hard spheres confined between two concentric shells. These systems are

*antoine@lptmc.jussieu.fr
†talbot@lptmc.jussieu.fr

dominated by ballistic and diffusive transport at low and high densities, respectively. The hard particles collide elastically with each other and with the boundaries and follow rectilinear trajectories at a constant velocity between collisions. The inner circle or sphere constitutes a target. We examine the passage times of activated particles from the outer wall to the target, as well as the reverse process of deactivated particles from the inner to the outer boundary using a "color" labeling scheme detailed below. We consider the reaction in this system to be the arrival of activated particles at the target. Like the lattice model studied previously [15], our model incorporates crowding and confinement. Unlike this study, however, layering is present at sufficiently high densities.

We chose to examine hard-particle fluids for two reasons. First, despite the simplicity of the (purely repulsive) interaction potential, the structure of these model fluids matches closely that of real fluids in which attractive interactions are also present. Second, the transport properties of the bulk fluids are well known at intermediate and high densities, and accurate interpolation formulas are available that cover the entire density range.

The outline of the paper is as follows. In Sec. II, we detail the model and the simulation methodology. In Sec. III, we present simulation results for the steady-state reaction rate and the MFPTs and their ratio. Insight into the system dynamics is provided by examining the particle trajectories at different packing fractions. In the following sections we present a quantitative approach to the ballistic (Sec. V) and diffusive (Sec. IV) regimes. In Sec. VI we propose a Bosanquet-like approach with a view to providing a global description of the reaction rate. Finally, we present preliminary results for the position dependence of the diffusion coefficient in Sec. VII. Section VIII reports our conclusions.

II. MODEL AND SIMULATION

The 2D model system consists of N hard disks of diameter σ confined in an annulus of inner and outer radii R_0 and R_1, respectively, corresponding to a packing fraction

$$\eta = \frac{N\sigma^2}{4\left(R_1^2 - R_0^2\right)}. \tag{1}$$

In a bulk system of hard disks, the solid-fluid coexistence region lies between $0.699 < \eta < 0.723$ [34,35] and the maximum packing fraction is $\eta_{\max} = \pi/(2\sqrt{3}) = 0.907$ for a close-packed hexagonal solid.

In the 3D system of N hard spheres of diameter σ confined between concentric shells of inner and outer radii R_0 and R_1, respectively, the packing fraction is

$$\eta = \frac{N\sigma^3}{8\left(R_1^3 - R_0^3\right)}. \tag{2}$$

In the bulk hard-sphere system there is a first-order transition with a coexistence region between $0.492 < \eta < 0.545$ and, at close-packing, $\eta_{\rm cp} = \pi/(3\sqrt{2}) = 0.740$.

The hard particles undergo elastic collisions with each other and with the walls so that the total energy

$$E = \frac{1}{2}\sum_{i=1}^{N} m v_i^2 \tag{3}$$

is constant. Since the collisions with the wall are specular, the angular momentum

$$\boldsymbol{L} = \sum_{i=1}^{N} \boldsymbol{r}_i \times m\boldsymbol{v}_i \tag{4}$$

is also a conserved quantity, while the linear momentum is not. Between collisions the particles follow rectilinear trajectories. When the number of confined particles is small, the statistical properties of the system depend strongly on the total angular momentum [36,37]. In this study all the reported results are for $L = 0$. The particle behavior is similar for $L = 0$ and a random distribution of L with zero mean only if N is large enough. For very small values of N, some particular initial configurations may lead to situations where the particles may not collide each other or with the inner annulus or shell. In these cases, τ_1, τ_0, and Γ may not possess a well-defined (mean) value. The trajectories were obtained numerically using the standard event-driven molecular dynamics (MD) algorithm [38]. Since the interaction is hard core there is no potential energy, and increasing the temperature is equivalent to speeding the system up. More specifically, the time scales as $\sqrt{T}$, where T is the temperature. For convenience we take $k_BT/m = 1$, where k_B is the Boltzmann constant and m the mass of the disk or sphere.

The initial configurations were generated by placing particles randomly without overlap between the confining walls. The velocities were then rescaled to remove the total angular momentum and impose that $E/m = k_BT/m = 1$ (see Appendix D). The system is allowed to equilibrate until a steady state is obtained.

To investigate the effect of self-crowding on the dynamics we consider the first-passage times between the inner and the outer walls using a color labeling scheme [39]. Particles are labeled either blue (activated) or red (deactivated). When a blue particle touches the inner boundary, or target, it is deactivated (and becomes red). See Fig. 1. We use τ_1 to denote the mean first-passage time of this process, i.e., the time elapsed between the activation of a particle to its deactivation. Similarly, τ_0 denotes the MFPT associated with the passage from the inner to the outer boundary, deactivated $\rightarrow$ activated. These quantities are averaged over a large number of long (typically $>10^6$ collisions per particle), independent runs, each starting from a different random configuration.

Because of the system geometry, these two MFPTs are not the same, as is the case for a slit pore. After a transient period the composition of the system, i.e., the fraction of activated particles, fluctuates around a steady-state value. Note that, particularly at high densities, the steady state of the color reaction is attained much more slowly than other properties such as the velocity distribution.

We also examine a reaction rate associated with the MFPTs. More specifically, let Γ denote the mean number of activated (blue) particles colliding with the target (inner wall) per unit time. In the steady state the reaction rate is related to the

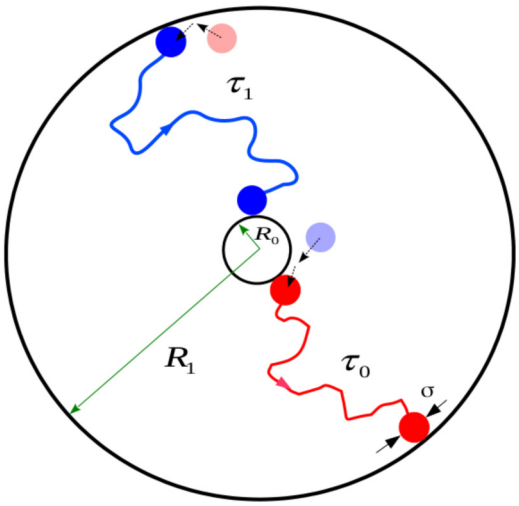

FIG. 1. The 2D system consists of N hard disks of diameter σ confined between an annulus of inner and outer radii R_0 and R_1, respectively. Disks are labeled either blue (activated) or red (deactivated). A blue disk becomes red when it touches the inner boundary (target) and a red disk becomes blue when it touches the outer boundary. The MFPT τ_1 is the mean time between activation and deactivation (a complete trajectory of a blue particle), while τ_0 is the mean time between deactivation and activation (a complete trajectory of a red particle).

MFPTs as follows:

$$\Gamma = \frac{N}{\tau_0(\eta) + \tau_1(\eta)}. \tag{5}$$

III. PHENOMENOLOGY

In this section we provide a preliminary overview of the simulation results. More detailed analysis is reserved for later sections after the necessary theory is introduced.

Figure 2 shows a snapshot of a dense system in the steady state. There are substantially more blue particles than red ones, with the latter being largely confined to a region around the target. At this relatively high packing fraction (0.635), the presence of layers is clearly visible next to the outer wall. The onset of layering can be quantified by examining the radial density at different packing fractions as shown in Fig. 3. At a low bulk density the radial density varies little with distance, but marked oscillations appear as the number of confined particles increases. The local density is maximum next to the outer wall and there is another strong maximum at the inner wall. At moderate densities the local density is nearly constant in the middle region, but ordering finally propagates into this region as the particle number increases.

Figures 4 and 5 show the reaction rate of confined hard disks as a function of the packing fraction in the steady state computed from simulation for different geometries of the annulus. The reaction rate initially increases with an increasing number of particles but then decreases due to self-crowding effects, leading to a maximum value at an intermediate packing fraction. The more confined the system, the more pronounced the maximum in the reaction rate (sharper and more intense). As the system size increases, the maximum shifts slowly to

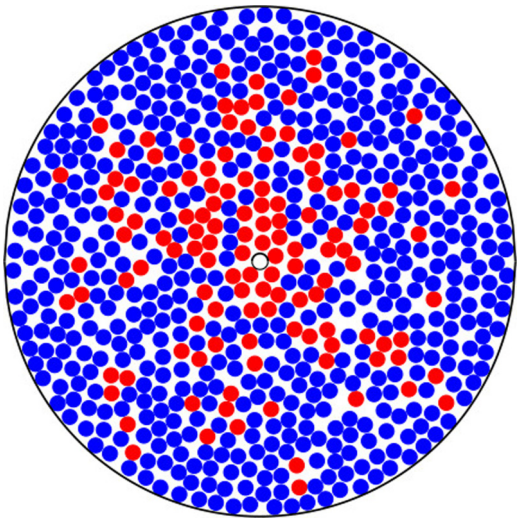

FIG. 2. A configuration in the steady state for a system of hard disks with $R_1 = 16$, $R_0 = 0.5$, $N = 650$ ($\eta = 0.635$). The presence of layering is clearly evident at this density.

higher packing fractions. We also note the crossing of the curves on the right-hand side. As we argue later, this effect cannot be explained by assuming a Smoluchowski model with uniform diffusivity. The 3D system of hard spheres confined between two concentric shells shows a similar behavior. See Fig. 6.

Figure 7 shows τ_1 as a function of the packing fraction for three geometries in two dimensions. At very low packing fractions there are few disk-disk collisions and the particles are constrained by the $L = 0$ condition to go directly back and forth between the inner and the outer boundaries. This results in a small τ_1. As the density increases, the increasing frequency of disk-disk collisions leads to a rapid increase in the MFPT. Even after the initial extremely rapid increase we observe a

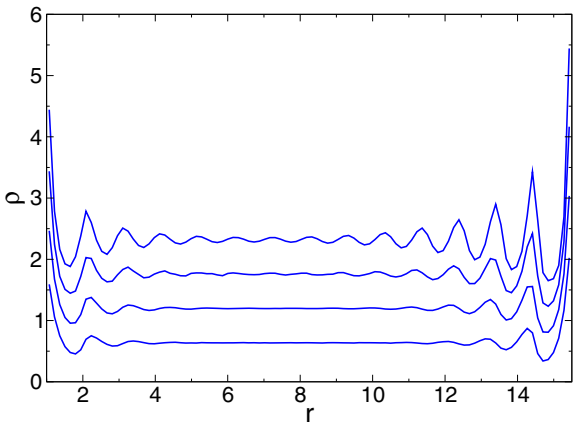

FIG. 3. Radial density of N hard disks in an annulus of radii $R_0 = 0.5$ and $R_1 = 16$ for $N = 500$, 550, 600, and 650, from bottom to top (corresponding packing fractions: $\eta = 0.196$, 0.392, 0.510, and 0.588, respectively). For clarity, the curves for $N = 550$, $N = 600$, and $N = 650$ are displaced in the vertical direction by 0.5, 1, and 1.5 units, respectively. The layering effect is most intense next to the outer wall.

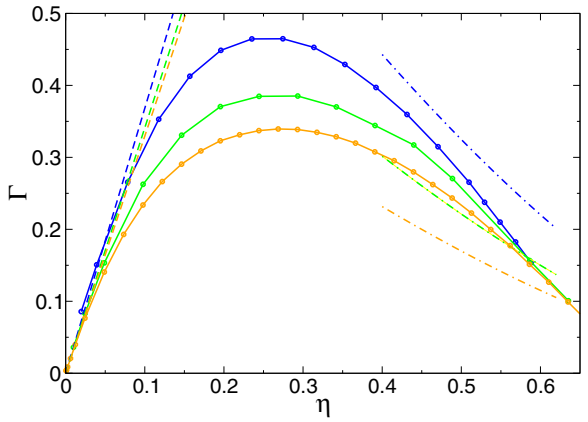

FIG. 4. Reaction rate of confined hard disks (2D) in the steady state as a function of the packing fraction. $R_0 = 0.5$ (top) and $R_1 = 8$, $R_1 = 16$, and $R_1 = 32$ (from top to bottom). Dashed lines show the predictions of the ballistic regime theory, Eq. (26); dashed-dotted lines, the predictions of the Smoluchowski theory, Eq. (9), with the Enskog diffusion coefficient.

superexponential dependence on the packing fraction that is the direct result of crowding.

Figure 8 shows the ratio of the MFPTs, τ_1/τ_0. Except at very low packing fractions this is a decreasing function of the packing fraction. For moderate values of η the ratio attains a nearly constant value. We attribute the sharp drop-off at small packing fractions to the imposition of zero total angular momentum. This condition implies strong constraints on the dynamics when there are few particles. For example, when $N = 1$, it imposes that $\tau_1/\tau_0 = 1$, but for $N = 2$, it tends to decrease the probability of a disk's directly hitting the target from the initial random configuration of positions and velocities. For $N \geqslant 2$, the system is chaotic and the disks always end up colliding with the inner wall.

In Fig. 9 we show some sample trajectories for systems of different packing fractions. Four regimes can be identified:

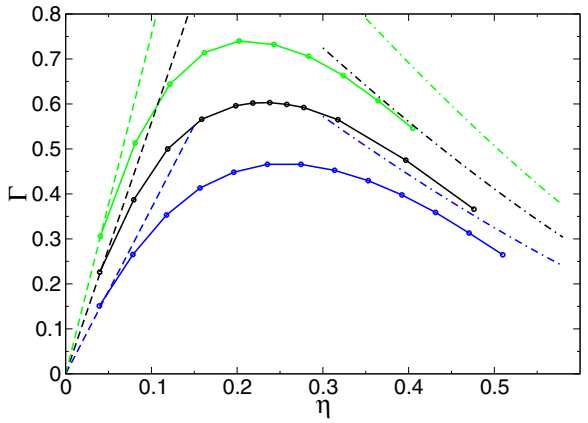

FIG. 5. Reaction rate of confined hard disks (2D) in the steady state as a function of the packing fraction for $R_1 = 8$ and, from top to bottom, $R_0 = 1.5$, 1, and 0.5. Dashed lines show the predictions of the ballistic regime theory, Eq. (26); dashed-dotted lines, the predictions of the Smoluchowski theory, Eq. (9), with the Enskog diffusion coefficient.

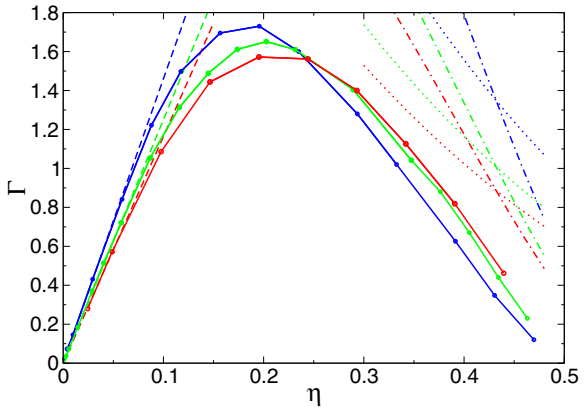

FIG. 6. Reaction rate of confined hard spheres in the steady state as a function of the packing fraction for various values of the external boundary radius R_1 (with a constant internal boundary $R_0 = 0.5$). From top to bottom (on the left): $R_1 = 4$, $R_1 = 6$, and $R_1 = 8$. Dashed lines show the predictions of the kinetic theory, Eq. (30). Also shown are the predictions of the Smoluchowski theory, Eq. (14), with a constant diffusion coefficient using the results of the Enskog theory (dotted lines) and Enskog theory with the correction proposed by Heyes *et al.* (dash-dotted lines) [41].

(i) At very low particle numbers, the dynamics is clearly dominated by ballistic trajectories. Disk-disk collisions are rare and a particle typically collides many times with the walls before encountering another particle. As a consequence, τ_0 is of the order of $(R_1 - R_0 - \sigma)/\langle v \rangle$, where $\langle v \rangle$ is the mean velocity of the particles, whereas τ_1 is much larger since the probability of hitting the central target is low. (ii) For a slightly higher value of η, interparticle collisions cause τ_0 and τ_1 to increase, but also facilitate the collision of blue particles with the target, leading to a decrease in the ratio τ_1/τ_0. (iii) At higher densities, the trajectories are dominated by diffusive motion and τ_1/τ_0 tends to a constant value for a broad range of η. (iv) Finally, for very large packing fractions, τ_1/τ_0 tends to decrease with η due to the layering effect, which is more

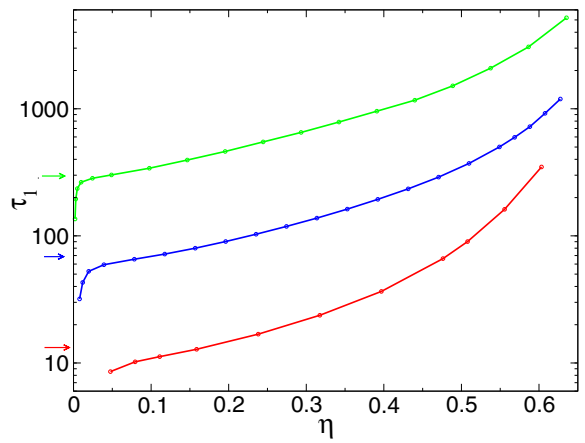

FIG. 7. MFPT for a particle to transit from the outer boundary at R_1 to the inner boundary (target) at R_0, τ_1, as a function of the packing fraction η in two dimensions. From top to bottom: $R_1 = 16$, $R_1 = 8$, and $R_1 = 4$ ($R_0 = 0.5$). Arrows show the prediction of the kinetic theory, Eq. (25).

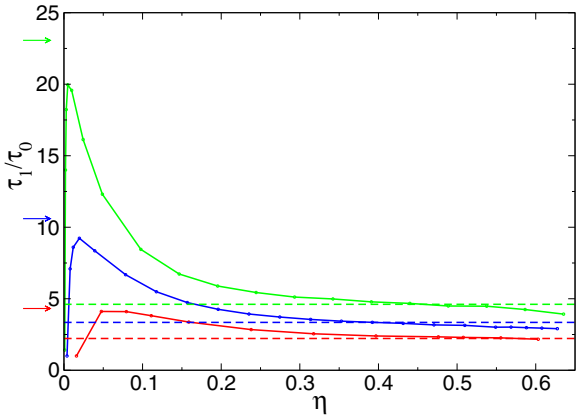

FIG. 8. Ratio of the MFPTs τ_1/τ_0 as a function of the packing fraction η for various values of the external boundary R_1 in two dimensions. From top to bottom: $R_1 = 16$, $R_1 = 8$, and $R_1 = 4$. Dashed lines correspond to the theoretical estimate, Eq. (10), within the diffusive approach and arrows show the predictions of the kinetic theory, Eq. (27).

pronounced near the outer wall (creating a higher barrier for red particles).

If the fluid density is not too low and the confinement not too strong, one can attempt to use the Smoluchowski equation within a diffusive approach to determine τ_0 and τ_1 [40]. For either a low density or a strong confinement the diffusive approach is no longer valid, as the dynamics are controlled by a wall-mediated ballistic regime. Note that this is distinct from a wall-mediated diffusive, or Knudsen, regime. In our system we assume specular reflections that prevent thermalization due to the collisions with the walls. The system geometry is thus expected to play a crucial role in determining both the mean distance traveled by the disks between the inner and the outer boundaries and the associated reaction probability.

Finally, we develop a global description of the kinetics by making use of a Bosanquet-like formula that effectively interpolates between the ballistic and the diffusive regimes. Some discrepancies are expected at intermediate and high densities due to the layering effects close to R_1 and R_0 that are not incorporated in the theoretical description.

IV. DIFFUSIVE REGIME

If we assume diffusive motion with a uniform coefficient of diffusion D_0, the mean first-passage time obeys the Poisson equation $D_0\nabla^2\tau(r|r_0,r_1) = -1$, where $\tau(r|r_0,r_1)$ denotes the MFPT for a particle starting from r with an absorbing boundary at r_0 and a reflecting boundary at r_1. The boundary conditions are $\tau(r_0|r_0,r_1) = 0$ and $\frac{d\tau(r|r_0,r_1)}{dr}|_{r=r_1} = 0$.

A. Two dimensions: Hard disks

In two dimensions, the solution of the Poisson equation with absorbing and reflecting boundary conditions is

$$\tau(r|r_0,r_1) = \frac{1}{D_0}\left[\frac{r_1^2}{2}\ln(r/r_0) - \frac{r^2}{4} + \frac{r_0^2}{4}\right], \quad (6)$$

from which we deduce

$$\tau_1 = \tau(r = r_1|r_0,r_1) = \frac{1}{D_0}\left[\frac{r_1^2}{2}\ln(r_1/r_0) - \frac{r_1^2}{4} + \frac{r_0^2}{4}\right], \quad (7)$$

and for the reverse process

$$\tau_0 = \tau(r = r_0|r_1,r_0) = \frac{1}{D_0}\left[\frac{r_0^2}{2}\ln(r_0/r_1) - \frac{r_0^2}{4} + \frac{r_1^2}{4}\right], \quad (8)$$

where we have introduced $r_0 = R_0 + \sigma/2$ and $r_1 = R_1 - \sigma/2$ to account for the finite size of the diffusing disks. We note that the system geometry leads to an asymmetry in the MFPTs (that is not present in a slit-pore system). From Eq. (5) we obtain a simple expression for the steady-state reaction rate:

$$\Gamma_{D_0} = \frac{2D_0N}{(r_1^2 - r_0^2)\ln(r_1/r_0)}. \quad (9)$$

The diffusion coefficient that appears in this equation is strongly density dependent. We can estimate it using known results for hard disks [42,43]. See Appendix A for the corrected Enskog expression of D_0. The approach is no longer valid when the mean free path exceeds the system size, i.e., when either the number of disks is very low or the confinement is very strong. Indeed, D_0 approaches a nonphysical infinite value for $\eta \longrightarrow 0$ (unlike colloid particles, for which the self-diffusion tends to a finite value in the low-density limit). This implies that the reaction times τ_1 and τ_0 cannot display a minimum for a particular system density or size in a purely diffusive description. In any case, we do not expect the Smoluchowski approach to be valid at low to intermediate densities [44].

Figures 4 and 5 show the comparison of Eq. (9) using the Enskog theory for D_0. The theory correctly predicts that the reaction rate decreases with increasing density, but the agreement is not quantitative. Using the corrected Enskog theory (Appendix B) does not improve the prediction, except at very high densities. This hints at the strong influence of confinement and layering, effects that are not taken into account in the modified Enskog theories.

Within the framework of the Smoluchowski theory with a constant coefficient of diffusion the ratio τ_1/τ_0 depends only on the system geometry,

$$\frac{\tau_1}{\tau_0} = \frac{2(r_1/r_0)^2\ln(r_1/r_0) - (r_1/r_0)^2 + 1}{(r_1/r_0)^2 - 2\ln(r_1/r_0) - 1}, \quad (10)$$

and converges slowly to $2\ln(r_1/r_0)$ for large values of r_1/r_0 due to the asymmetry between τ_1 and τ_0 when $r_1 \gg r_0$: τ_1 scales as $2r_1^2\ln(r_1/r_0)$, whereas τ_0 scales as r_1^2 only. Comparison with the simulation results shows that Eq. (10) is only valid in a narrow range of packing fractions. At high packing fractions it overestimates the ratio, while for small to intermediate packing fractions, the simulated ratio is much higher than predicted by the theory. In the latter regime where the friction is low, the Smoluchowski theory is no longer valid [44]. More quantitatively, the Stokes-Einstein relation in two dimensions implies that the diffusive time scale (inverse of the friction coefficient) scales as $(\pi D_0)/(k_BT)$ [45,46]. For the Smoluchowski approach to be valid for describing a process, this time scale must be much smaller than the duration of the process itself, namely, τ_0 in the present case. Due to confinement, τ_0 is larger than 1% of the diffusive time scale for

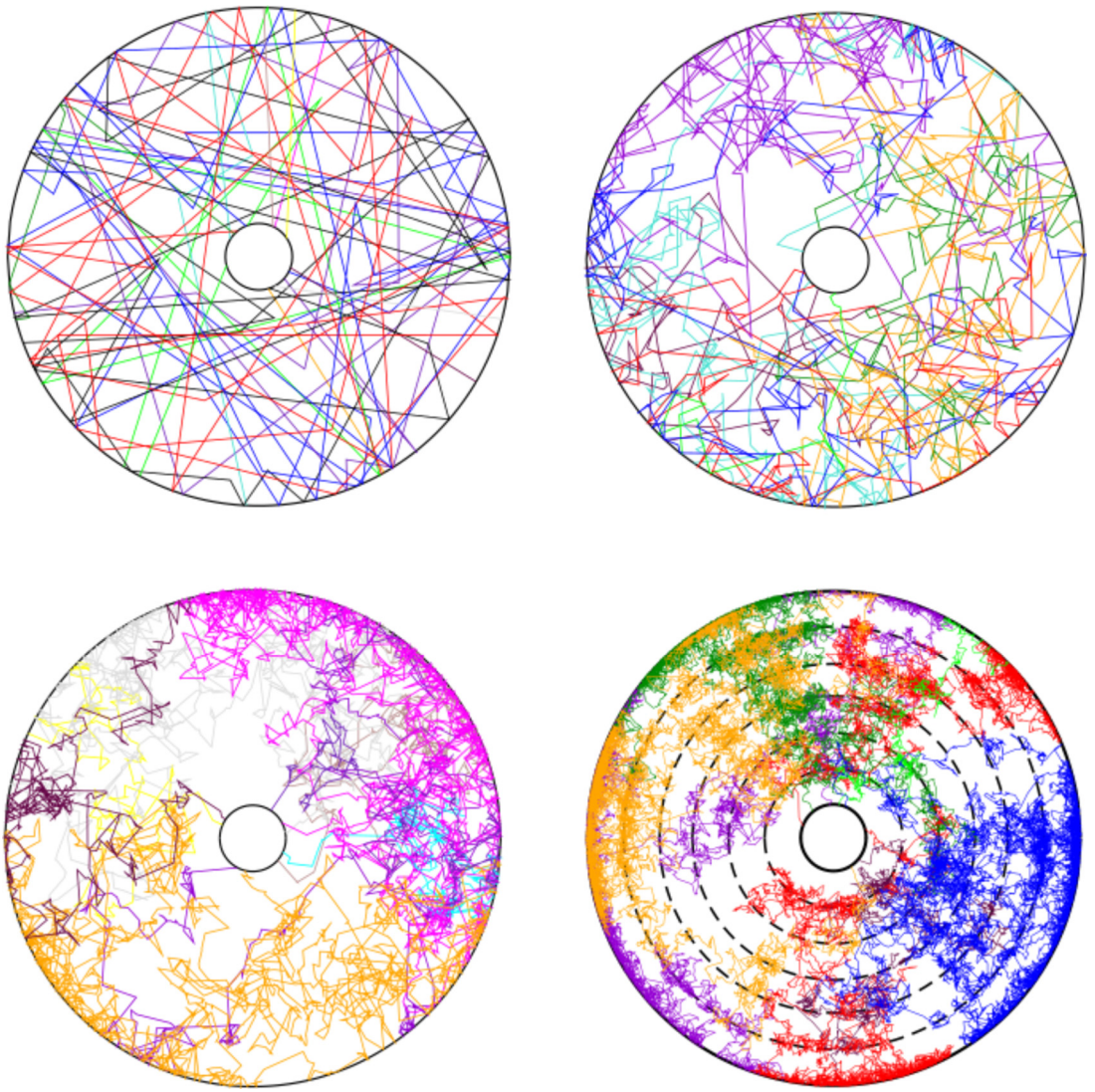

FIG. 9. Some illustrative first-passage trajectories of hard disks in an annulus with $R_0 = 0.5$ and $R_1 = 8$. Each line shows an independent trajectory for a particle starting in contact with the outer boundary until it reaches the inner (target) boundary. Left to right and top to bottom: $N = 5$ ($\eta = 0.02$), $N = 50$ ($\eta = 0.196$), $N = 100$ ($\eta = 0.392$), and $N = 150$ ($\eta = 0.588$). Inner and outer full circles of radii $R_0 + 0.5$ and $R_1 - 0.5$ show the limits of the disk centers. Dashed circles in the densest configuration show the locations of the maxima in the radial density.

the following configurations ($R_0 = 0.5$ in all cases): $\eta < 0.5$ if $R_1 = 4$, $\eta < 0.4$ if $R_1 = 8$, $\eta < 0.3$ if $R_1 = 16$, and $\eta < 0.2$ if $R_1 = 32$. These limiting values conform well with the crossovers observed between numerical data and theoretical predictions, Eqs. (7) and (8).

B. Three dimensions: Hard spheres

In a 3D system of hard spheres confined between two concentric shells the solution of the Poisson equation is

$$\tau_1 = \tau(r = r_1|r_0,r_1) = \frac{1}{3D_0}\left[r_1^3\left(\frac{1}{r_0} - \frac{1}{r_1}\right) + \frac{1}{2}\left(r_0^2 - r_1^2\right)\right], \tag{11}$$

$$\tau_0 = \tau(r = r_0|r_0,r_1) = \frac{1}{3D_0}\left[r_0^3\left(\frac{1}{r_1} - \frac{1}{r_0}\right) + \frac{1}{2}\left(r_1^2 - r_0^2\right)\right], \tag{12}$$

where D_0, the self-diffusion coefficient of hard spheres, can be approximated by a corrected Enskog expression (see Appendix B for more details).

The ratio of MFPTs is

$$\frac{\tau_1}{\tau_0} = \frac{1 + 2\beta^{-1}}{1 + 2\beta} \tag{13}$$

and the expression for the rate of reaction in the diffusive regime is

$$\Gamma_{D_0} = \frac{3D_0N}{r_0^2[\beta^{-2}(\beta^{-1} - 1) + \beta - 1]}. \tag{14}$$

Similarly to what was observed in the 2D system, this expression is unable to provide a quantitatively accurate description of the simulation results when D_0 is approximated by the Enskog theory or the corrected version, although the latter does a better job at high densities. See Fig. 6. Again, we

conclude that layering and confinement strongly influence the dynamics.

As for the composition of the system in the steady state, we can use the same approach as in two dimensions. Like the ratio τ_1/τ_0, it is independent of the diffusion coefficient. Details are given in Appendix C.

V. BALLISTIC REGIME

In this section we develop a kinetic theory for the reaction rate in the ballistic regime, i.e., for low to intermediate packing fractions, for which the diffusive (Smoluchowski) approach is expected to be invalid. For a small number of particles the dynamics is dominated by trajectories between the outer and the inner walls. The trajectory of a single particle can be defined by θ, the angle of incidence with respect to an inward normal on the outer wall (see Fig. 10). If $\theta < \theta_c$, where $\sin\theta_c = r_0/r_1$, a particle following this trajectory collides with the inner wall (target) at an angle of incidence ϕ. Elementary trigonometry shows that these angles are related by

$$r_0 \sin\phi = r_1 \sin\theta. \tag{15}$$

The distance traveled by the particle between two consecutive collisions with the outer and inner walls is

$$x^*(\phi) = \sqrt{1-\beta^2\sin^2\phi} - \beta\cos\phi \tag{16}$$

in terms of ϕ and

$$x^*(\theta) = \cos\theta - \sqrt{\beta^2 - \sin^2\theta} \tag{17}$$

in terms of θ. Distances have been adimensioned with r_1, $x^* = x/r_1$, and

$$\beta = r_0/r_1. \tag{18}$$

If $\theta > \theta_c$, the particle misses the target and recollides with the outer wall, and the distance traveled between two consecutive collisions is $x^*_{\rm miss} = 2\cos\theta$.

We now consider the situation with more than one particle. If N is not too small, the dynamics consists primarily of ballistic trajectories between the walls, occasionally interrupted by collisions with another disk. For a semi-infinite ideal gas next to a planar wall the incidence angle, ψ, is distributed as $\cos\psi$. For example, for the system $R_0 = 0.5, R_1 = 8$, simulations in two dimensions show that this is the case for the angle ϕ for all values of N and is adequate for θ for $N \gtrsim 10$ (see Fig. 11).

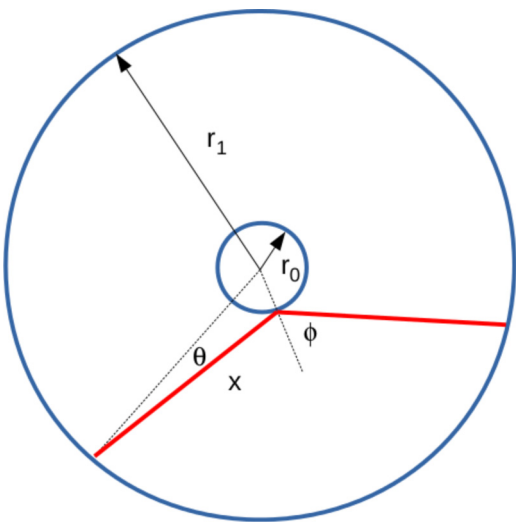

FIG. 10. Geometric quantities for ballistic trajectories.

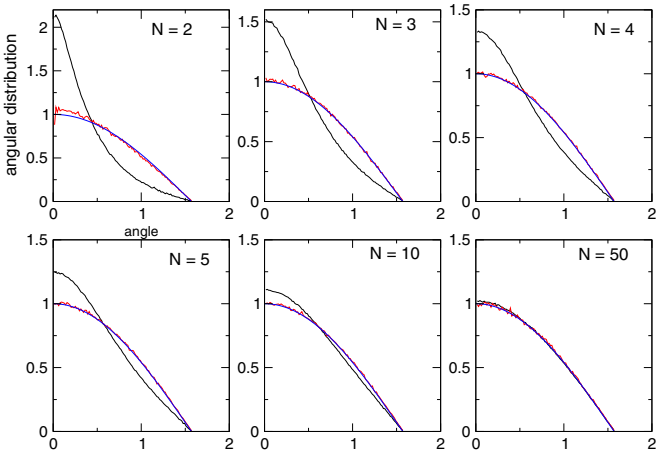

FIG. 11. Distribution of the takeoff angles θ (black lines) and ϕ (red lines) (see Fig. 10) for different numbers of hard disks in an annulus of dimensions $R_0 = 0.5$ and $R_1 = 8$. The blue line shows $\cos\theta$, the expected result for a bulk ideal gas colliding with a planar wall.

A. Two dimensions: Hard disks

Let us first consider a particle leaving the inner wall. It will collide with the outer wall regardless of the takeoff angle ϕ (assuming that it does not first collide with another disk).

Assuming a cosine distribution [29,31,33] we find that the average (adimensioned) length traveled by such a disk before collision with the outer wall is

$$x_0^* = \int_0^{\pi/2} x^*(\phi)\cos(\phi)d\phi = -\frac{\beta\pi}{4} + \frac{\sqrt{1-\beta^2}}{2} + \frac{\arcsin\beta}{2\beta}. \tag{19}$$

For $\beta < 1$ a Taylor-series expansion yields

$$x_0^* = 1 - \frac{\pi}{4}\beta - \frac{\beta^2}{6} + O(\beta^3). \tag{20}$$

We estimate the average time to reach the outer wall as $\tau_{0b} = x_0(\beta)/\langle v\rangle$, where $\langle v\rangle = \sqrt{\frac{\pi}{2}\frac{k_BT}{m}}$ is the mean velocity of a 2D gas.

Now consider a particle rebounding from the outer wall at a normal angle θ. The probability of hitting the target is

$$p_{\rm hit} = \int_0^{\theta_c} \cos(\theta)d\theta = \beta. \tag{21}$$

If $\theta < \theta_c$, the particle collides with the inner wall and the average distance traveled is

$$x^*_{\rm hit} = \int_0^{\theta_c} x^*(\theta)\cos(\theta)d\theta \Big/ \int_0^{\theta_c}\cos(\theta)d\theta$$
$$= -\frac{\pi\beta}{4} + \frac{\arcsin(\beta)}{2\beta} + \frac{\sqrt{1-\beta^2}}{2} = x_0^*. \tag{22}$$

If $\theta > \theta_c$, the particle misses the target and travels an average distance

$$x^*_{\rm miss} = \int_{\theta_c}^{\pi/2} 2\cos^2(\theta)d\theta \Big/ \int_{\theta_c}^{\pi/2} \cos\theta d\theta = \frac{\arccos(\beta) - \beta\sqrt{1-\beta^2}}{1-\beta} \tag{23}$$

before recolliding with the outer wall. The target may be hit directly or after k rebounds. Assuming that the successive takeoff angles are uncorrelated we estimate

$$\tau_1 = \sum_{k=0}^{\infty}(1-p_{\rm hit})^k p_{\rm hit}(kt_{\rm miss} + t_{\rm hit}), \tag{24}$$

where, e.g., $t_{\rm hit} = x_{\rm hit}/\langle v\rangle$. Evaluating the sum yields

$$\tau_1 = t_{\rm hit} + \left(\frac{1-\beta}{\beta}\right)t_{\rm miss}. \tag{25}$$

From Eq. (5) we estimate the rate of reaction in the ballistic regime as

$$\Gamma_b = \frac{\sqrt{8\pi}\left(R_1^2 - R_0^2\right)}{r_1(x_0^* + x_{\rm hit}^* + (1/\beta - 1)x^*_{\rm miss})}\eta = \frac{\sqrt{8\pi}\left(R_1^2 - R_0^2\right)}{r_1}\beta\left[\frac{2}{\pi} + O(\beta)\right]\eta, \tag{26}$$

where we have set $k_BT/m = 1$ as in the simulations. This formula is in good agreement with the simulation results (see Figs. 4 and 5). Similarly, the ratio of the MFPTs can be obtained as

$$\frac{\tau_{b1}}{\tau_{b0}} = \frac{x_{\rm hit}^* + (1/\beta - 1)x^*_{\rm miss}}{x_0^*} = \frac{\pi}{2\beta} + \frac{\pi^2}{8} - 1 + O(\beta). \tag{27}$$

This expression conforms well with the small packing fraction peak of τ_1/τ_0 (see Fig. 8) but naturally underestimates the value of MFPTs since the above calculations do not account for disk-disk collisions. The increase in the path length due to these collisions can be simply implemented by assuming the independence of the collisions and considering a sum similar to Eq. (24). We do not, however, develop these calculations here, as they require us to make assumptions about the distribution of disk-disk collision angles.

B. Three dimensions: Hard spheres

In the ballistic regime $p_{\rm hit} = \beta^2$ and the mean velocity $\langle v\rangle = \sqrt{8k_BT/(\pi m)}$. The average (adimensioned) distances are

$$x_0^* = x_{\rm hit}^* = \frac{2}{3\beta^2}(1 - \beta^3 - (1-\beta^2)^{3/2}) \tag{28}$$

and

$$x^*_{\rm miss} = \tfrac{4}{3}\sqrt{1-\beta^2}, \tag{29}$$

leading to the expression for the ballistic reaction rate

$$\Gamma_b = \frac{8\sqrt{8/\pi}\left(R_1^3 - R_0^3\right)}{r_1(x_0^* + x_{\rm hit}^* + (1/\beta^2 - 1)x^*_{\rm miss})}\eta = \frac{8\sqrt{8/\pi}\left(R_1^3 - R_0^3\right)}{r_1}\left(\frac{3}{4}\beta^2 + O(\beta^4)\right)\eta, \tag{30}$$

and the ratio of the MFPTs is given by

$$\frac{\tau_{b1}}{\tau_{b0}} = \frac{x_{\rm hit}^* + (1/\beta^2 - 1)x^*_{\rm miss}}{x_0^*} = \frac{4}{3\beta^2} + \frac{8}{9\beta} - \frac{2}{27} + O(\beta). \tag{31}$$

Figure 6 shows that the kinetic theory, Eq. (30), provides an accurate description of the simulation at low densities. The Smoluchowski theory, Eq. (14), with a uniform diffusion coefficient, describes only qualitatively the behavior of $\Gamma(\eta)$ at very high densities. Going beyond the Enskog theory by accounting for the hydrodynamic and finite-size effects (as did Heyes *et al.* [41]) simply amounts to getting better slopes at high densities. At intermediate to high densities, neither the ballistic nor the diffusive regime is able to account for the particular bell shape of $\Gamma(\eta)$ for such self-crowding systems.

VI. BOSANQUET APPROACH

Several formulas have been proposed to account for these different (ballistic and diffusive) regimes over the whole density range [30,47,48]. Assuming that the frequencies of various kinds of collisions are additive, Bosanquet developed a particularly simple interpolation formula for the global diffusion coefficient D,

$$\frac{1}{D} = \frac{1}{D_K} + \frac{1}{D_0}, \tag{32}$$

which has proved to be accurate to a few percent [30,49].

In this expression, D_K is the diffusion coefficient corresponding to the Knudsen regime, obtained for strong confinement and diffusive wall-particle interactions [29,30]. For hard disks, for example, *if* the wall-disk interactions were diffusive, the Knudsen diffusion coefficient for our particular geometry would be given by $D_K = \frac{2}{\pi}v\lambda_K$, with the Knudsen mean free path [50,51] $\lambda_K = \frac{\pi\mathcal{A}}{\mathcal{P}} = \frac{\pi}{2}(r_1 - r_0)$, where $\mathcal{A}$ and $\mathcal{P}$ are, respectively, the area and perimeter of the 2D zone where the Knudsen regime would take place.

It is interesting to compare λ_K with the mean free path $\lambda_{\rm 2D}$ of a 2D Boltzmann gas [52]: $\lambda_{\rm 2D} = \frac{\pi\sigma}{8\sqrt{2}\eta g_2(\eta)}$. As is well known, $\lambda_{\rm 2D}$ diverges when η approaches 0, whereas λ_K does not depend on the packing fraction. On the other hand, $\lambda_{\rm 2D}$ does not depend on the system geometry, contrary to λ_K, which decreases with R_1. Consequently, as noted previously, the Boltzmann mean free path $\lambda_{\rm 2D}$ may become larger than λ_K if the confinement is too strong or if the density is too low, thereby invalidating the use of the Smoluchowski equation.

To devise a global expression for $\Gamma(\eta)$, we follow the approach of Bosanquet [19,20,47,49] by assuming that the frequencies of the ballistic and diffusive collisions are additive:

$$\frac{1}{\Gamma_{\rm Bos}} = \frac{1}{\Gamma_b} + \frac{1}{\Gamma_{D_0}}. \tag{33}$$

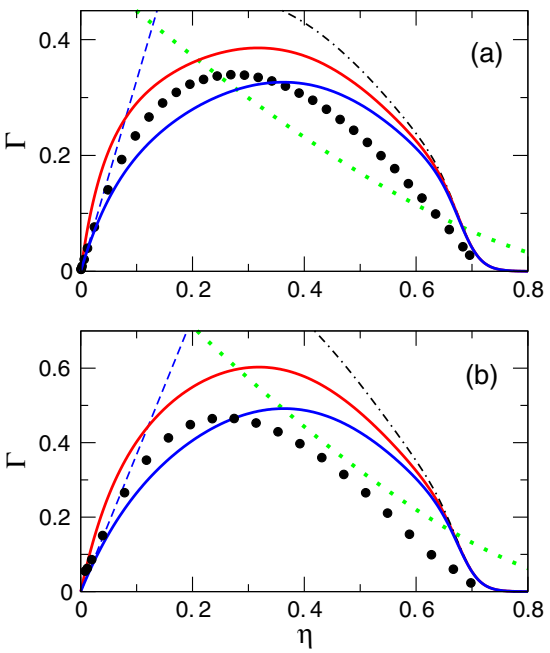

FIG. 12. Steady-state reaction rate, Γ, as a function of the packing fraction η for (a) $R_1 = 32$ and (b) $R_1 = 8$ in two dimensions (with a constant internal boundary $R_0 = 0.5$). Black circles: $\Gamma(\eta)$ from MD simulation. Solid lines: $\Gamma(\eta)$ from the Bosanquet-like formula Eq. (33), with D_0 from [43]. From bottom to top: blue lines, for Γ_b given by Eq. (26); and red lines, for $\Gamma_{b,N=2}$ (see text). Dashed blue line: Γ_b given by Eq. (26). Black dot-dashed line: diffusive reaction rate, Eq. (9), with D_0 from [43] (see Appendix A). Green dotted line: Enskog diffusive reaction rate.

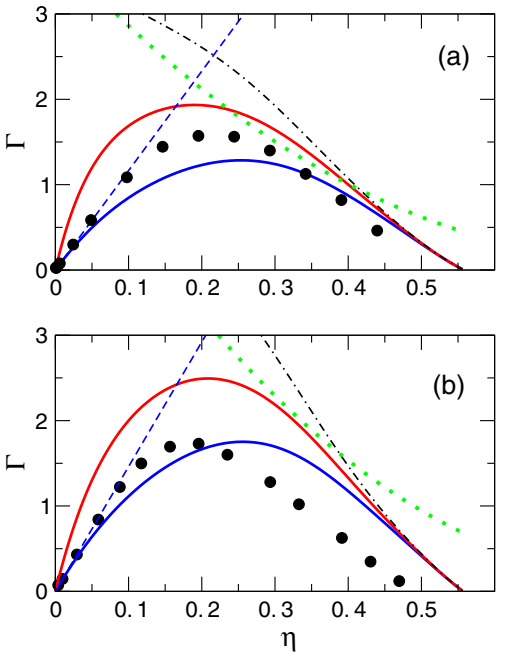

FIG. 13. Steady-state reaction rate Γ as a function of the packing fraction η for (a) $R_1 = 8$ and (b) $R_1 = 4$ in three dimensions (with a constant internal boundary $R_0 = 0.5$). Black circles: $\Gamma(\eta)$ from MD simulation. Solid lines: $\Gamma(\eta)$ from the Bosanquet-like formula, Eq. (33), with D_0 from [41] (see Appendix B). From bottom to top: blue lines, for Γ_b given by Eq. (30); and red lines, for $\Gamma_{b,N=3}$ (see text). Dashed blue line: Γ_b given by Eq. (30). Black dot-dashed line: diffusive reaction rate, Eq. (14), with D_0 from [41] (see Appendix B). Green dotted line: Enskog diffusive reaction rate.

This amounts to rewriting Γ_b as in Eq. (9) with a *hypothetical* Knudsen diffusion coefficient D_{bK} defined as $D_{bK} = \frac{(r_1^2 - r_0^2)\ln(r_1/r_0)}{2(\tau_{0b}+\tau_{1b})}$. Let us emphasize that, in the present work, a Knudsen regime is not present since the disk-wall collisions are specular. Consequently, the ballistic regime described in Sec. V cannot strictly correspond to this Knudsen regime. Nevertheless, it can be seen as a useful, limiting behavior within the Bosanquet approach. Another limiting behavior can be contemplated by considering the ballistic value of $\Gamma_{b,N=2}$, obtained for the smallest relevant value of N, i.e., $N = 2$ in two dimensions, for which the distribution of the takeoff angle θ significantly deviates from the cosine distribution (see Fig. 11), and relation (24) is no longer valid since the wall-disk collisions are highly correlated. If it existed, the Knudsen reaction rate would be expected to lie between these two extreme values, Γ_b and $\Gamma_{b,N=2}$.

In Fig. 12 we show $\Gamma(\eta)$ and $\Gamma_{\rm Bos}(\eta)$ for weak ($R_1 = 32$) and strong ($R_1 = 8$) confinement in two dimensions. Two kinds of Bosanquet formulas have been considered: the first one (in blue) for Γ_b given by Eq. (26) and the other (in red) for $\Gamma_{b,N=2}$. These account well for the reaction rate maximum and bound the numerical MD values (black circles) at low to moderate densities, as expected. The agreement with numerical data is relatively good at low densities whatever the confinement but is only qualitative beyond $\eta = 0.2$ for strong confinement. Also shown are the ballistic reaction rate, Eq. (26), and the diffusive reaction rate, Eq. (9), with D_0 given either by the Enskog expression or by the modified Enskog expression from [41]. We clearly see that the density and finite-size effects cannot be ignored (see Appendix A), especially at high densities, where there is a nonphysical crossover between the Enskog diffusive reaction rate and the numerical MD values.

In Fig. 13 we show predictions obtained using the Bosanquet approach in three dimensions. As in two dimensions, we used the limiting formulas: the first one (in blue) for Γ_b given by Eq. (30) and the other (in red) for $\Gamma_{b,N=3}$ (the value $N = 3$ being the smallest N value for which the hard-sphere trajectories are truly 3D when the total angular momentum is null). The expression of the 3D diffusion coefficient D_0 is given by Eq. (B3) (see Appendix B) and accounts for hydrodynamics and finite-size effects. We draw the same conclusions as for the hard-disk systems, the global agreement being better when the confinement is reduced.

The discrepancy between the theoretical (with Γ_{D_0}) and the simulation results confirms that the confinement effects are not well captured by a model with a *uniform* diffusion coefficient. As previously noted, the confining boundaries induce a layer structure in their vicinity which may drastically reduce the *local* self-diffusion coefficient, driving up the mean passage times τ_0 and τ_1 and reducing Γ accordingly. As a first approximation we can consider the system as being composed of three annular regions: two quasicrystalline layered parts near R_1 and R_0, surrounding an effective "bulk" phase. A

higher density can be associated with the two layered parts, whereas the bulk density is accordingly reduced compared with that of the (ideal) nonlayered system. While the times τ_i are slightly reduced by the bulk phase, they are greatly enhanced by the two layered parts, which act like "molasses" on the incoming or departing particles. Another consequence of this layering is that it effectively creates a repulsive potential close to the boundaries at R_1 and R_0 that incoming particles have to overcome, leading to a further increase in the times τ_i. In Fig. 2 one can observe a few red disks that are effectively blocked from approaching the outer boundary by a dense layer of blue disks.

VII. POSITION-DEPENDENT DIFFUSIVITY

Similarly to what has been done above at low packing fractions, one can also question the application of the Smoluchowski approach leading to Eq. (9) since the necessary conditions for it to be valid may not be fulfilled at high η. As recalled in Refs. [53,54], these conditions are the following: (i) the target must be fixed at the center of the system; (ii) the reactive disks must not interact; and (iii) the dynamics of the disks must be purely diffusive and Markovian.

The first condition is respected here since r_0 acts as the main target of the problem (τ_1, the time needed to reach r_0 from r_1, is usually much larger than τ_0, the time needed to reach r_1 from r_0). The second condition is also respected since the only disk-disk interaction is the hard-core one, which is accounted for in the self-diffusion coefficient D_0.

The third condition is more complex to assess. It has been shown in Ref. [55] that a condition equivalent to (iii) is that the space and time variations of both the potential energy and the diffusion coefficient must be negligible on the scale of the characteristic length $\sqrt{m/(k_BT)}D_0$. As a consequence, the higher the density, the smaller this length, and the Smoluchowski equation may lose its validity because of the density oscillations due to the layering, which is characterized by a length scale approximately equal to σ, the hard-particle diameter. Since the diffusion coefficient D_0 is smaller than $\sqrt{k_BT/m\sigma}$ for packing fractions η higher than 0.2, the Smoluchowski approach with a uniform diffusion coefficient is not rigorously relevant for describing the disk dynamics in layered areas where η exceeds this value.

In bulk, dense, homogeneous fluids, diffusion coefficients can be estimated from the mean-squared displacement. But in confined environments it is not clear how to calculate the diffusion coefficient. In a slit pore, for example, motion parallel to the walls is diffusive. One can then use the mean-squared displacement to evaluate $D_\parallel$. But in the transverse direction the confining boundaries and the spatially varying density profile prevent the use of the mean squared displacement route to the diffusion coefficient $D_\perp$. Mittal *et al.* [21] studied the diffusive dynamics of a hard-sphere fluid confined between parallel walls. They determined the position-dependent collective diffusion coefficient normal to the walls using a Bayesian inference method. Surprisingly, they observed that it is larger in regions of a high local packing density, whereas D is a monotonically decreasing function of the density in the bulk fluid.

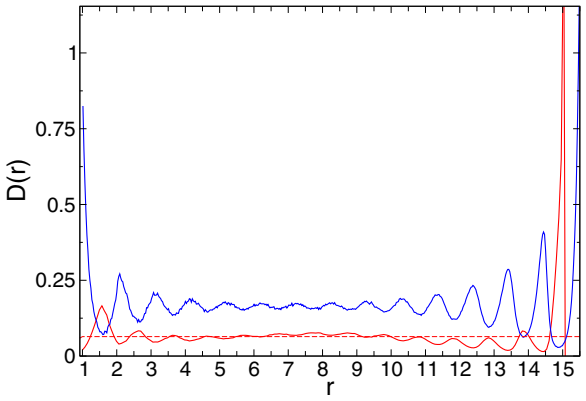

FIG. 14. Radial density (blue) and position-dependent diffusivity $D(r)$ (red) computed from Eq. (36) for a 2D system with $R_0 = 0.5$, $R_1 = 16$, and $N = 650$ ($\eta = 0.6354$). The dashed line shows the bulk diffusivity computed from the Enskog theory.

To properly account for the layering effect in a dense, confined system it is necessary to introduce a position-dependent diffusivity: either by using a simple model with shells with different diffusion coefficients [56,57] or by considering a heterogeneous Smoluchowski equation with a position-dependent diffusion coefficient. We now present some preliminary results for the latter case.

If the diffusion coefficient is taken as position dependent, the MFPT for a particle starting from r to reach the target at r_0 is given by

$$\tau_1(r) = \int_{r_0}^{r} \frac{dx}{D(x)p_{\rm eq}(x)} \int_x^{r_1} dy\ p_{\rm eq}(y), \tag{34}$$

where $p_{\rm eq}(r)$ is the equilibrium density at radial position r [40].

Now let $\psi(x) = \int_x^{r_1} dy\ p_{\rm eq}(y)$ so that the first-passage time becomes

$$\tau_1(r) = -\int_{r_0}^{r} \frac{dx}{D(x)\frac{d\ln\psi(x)}{dx}}, \tag{35}$$

where $\tau_1(r)$ is the MFPT for a particle to reach the inner boundary starting from r. Differentiating with respect to r yields

$$\frac{1}{D(r)} = -\frac{d\tau_1(r)}{dr}\frac{d\ln\psi(r)}{dr}. \tag{36}$$

This equation provides a route to the diffusion coefficient from the MFPTs and the densities determined in the simulations [58]. It is a simpler alternative to the Bayesian inference method of Hummer [59], but since it involves numerical derivatives it may be less accurate than that method.

We have applied this method to the dense system $R_0 = 0.5$, $R_1 = 16$, $N = 650$ (snapshot shown in Fig. 2). Figure 14 shows that $D(r)$ oscillates around the Enskog value and is *out of phase* with $\rho(r)$. That is, the diffusion coefficient is relatively large where the density is relatively low. This is seemingly consistent with the trajectories shown in Fig. 9, where the particle spends more time near the density maxima, but is in contradiction with the results of Mittal *et al.* [21] for a

slit pore. More extensive simulations are needed to understand the origin of this difference.

VIII. CONCLUSION

We have examined a simple model system of hard disks confined in annuli of varying sizes to investigate the effect of crowding and confinement on first passage times. The steady-state rate of the "color" reaction displays a maximum for a packing fraction between 0.2 and 0.3, depending on the system geometry. This is also observed in the corresponding 3D system of hard spheres confined between two concentric shells. It is interesting to note that in biological cells macromolecules typically occupy 20%–30% of the available volume [9]. In the ballistic regime at low densities the MFPTs and reaction rate are well described by a kinetic theory model. At higher densities we observe the onset of a diffusive regime that is only qualitatively described by a Smoluchowski-like theory with a constant coefficient of diffusion. The discrepancy is due, in part, to a layering phenomenon that becomes more and more pronounced with increasing density and confinement.

Surprisingly, the ratio τ_1/τ_0 is well described at intermediate and high densities by a formula assuming a constant diffusion coefficient, although neither τ_1 nor τ_0 is quantitatively well described by a diffusive approach which does not account for the layering effect. It may, however, be possible to capture the layering effect using a model with two or more shells with different diffusion coefficients [56,57] or within a Smoluchowski approach with a true position-dependent diffusivity.

We conclude that layering strongly affects the search for a target in a confined (self-)crowded medium since it hinders hard-core particles from reaching or leaving the confining boundaries. One can, however, imagine some situations where this effect might help a searcher to find a target more efficiently. For example, if the target is close to, or on, the boundary, the layering may facilitate the search.

APPENDIX A: DIFFUSION COEFFICIENT OF THE HARD-DISK FLUID

The diffusion coefficient D_0 that appears in Eqs. (6)–(9) refers to the self-diffusion coefficient of the hard-disk fluid of interest [60]. For infinite systems, this transport coefficient does not exist because of the well-known divergence of the long-time tail of the velocity autocorrelation function appearing in the Green-Kubo relation [61]. For finite systems, however, the asymptotic logarithmic tail is integrable and leads to a well-defined, finite value of the self-diffusion coefficient. It has even been shown that, in practice, this long-time tail problem is physically irrelevant for small enough systems like ours [62] and, consequently, can be ignored (or, at least, considered from the finite-size effects point of view; see below).

Like all diffusion coefficients, the self-diffusion coefficient is strongly density dependent and the usual Boltzmann-Enskog formula D_E has to be corrected by a factor $h(\eta)$ to account for the hydrodynamic and caging or crowding effects,

$$D_0 = D_E h(\eta) = \frac{\pi^{1/2}\sigma}{8\eta g_2(\eta)}\left(\frac{k_B T}{m}\right)^{1/2} h(\eta), \qquad \text{(A1)}$$

in the first Sonine approximation for D_E, and where the pair distribution function at contact $g_2(\eta)$ can be estimated using Henderson's equation, $g_2(\eta) = (1 - 7\eta/16)/(1 - \eta)^2$ [43], in two dimensions.

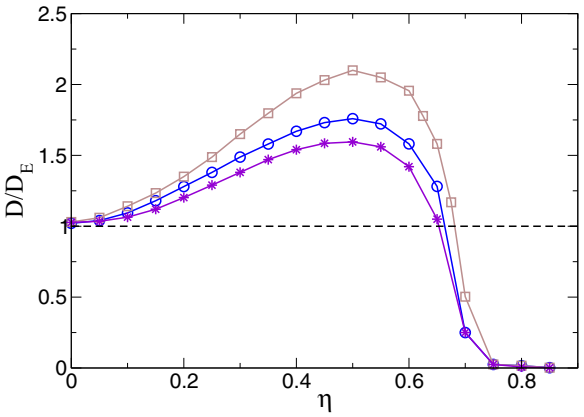

FIG. 15. Self-diffusion coefficients for hard-disk fluids from simulation scaled by the Enskog value. Adapted from Fig. 2 in Ref. [43]. These curves were obtained for a fixed number N of disks in a cell with periodic boundary conditions. Red squares and blue circles correspond to $N = 625$ and $N = 169$, respectively, and purple stars are associated with an $N \longrightarrow 0$ interpolation. Note that in the present study the area is kept fixed while the number of disks is varied, contrary to [43].

Even though the factor $h(\eta)$ does not qualitatively modify the behavior of $D_0(\eta)$—namely, a strong decrease with η and a divergence to infinity at $\eta = 0$—it may dramatically change its value at intermediate and high densities (by more than a factor of 2; see Fig. 15, adapted from Ref. [43]). No approximate analytical expression of $h(\eta)$ is known for the moment, although a polynomial expression has been numerically established for packing fractions below 0.5 [43]. Its zero density value is estimated as $h(0) \simeq 1.027$ in the ninth Sonine approximation [42]. For packing fractions below the Alder transition $\eta_c \simeq 0.7$, $h(\eta)$ is larger than 1 due to hydrodynamic effects, while for packing fractions above η_c, crowding and caging effects result in an abrupt collapse of D_0 compared with the smooth decrease in $D_E(\eta)$.

Finite-size effects have also been shown to greatly affect the factor $h(\eta)$ [42,43]. At a fixed density, in a square box with periodic boundary conditions, Garcia-Rojo *et al.* have shown [43] that the factor $h_N(\eta)$ increases in a nontrivial way with the number N of disks present in the simulation for $\eta \leqslant \eta_c$. In our case, it is pretty hard to estimate this size effect since (i) the total area $\pi(R_1^2 - R_0^2)$ of the system is obviously not relevant for the diffusion of disks between the r_1 and the r_0 boundaries; (ii) the system size is kept fixed, while it is the density that is varied; and (iii) the boundaries are not periodic and modify both the structure and the dynamics of the nearby hard-disk fluid.

One can nevertheless assume, in a first approximation, that the relevant number N' of disks corresponds roughly to the

disks contained in a virtual square box of side $R_1 - R_0$: $N' \simeq \frac{4(R_1-R_0)^2}{\pi\sigma^2}\eta$, finally yielding the self-diffusion coefficient $D_0 \simeq D_E h_{N'}(\eta)$.

APPENDIX B: DIFFUSION COEFFICIENT OF THE HARD-SPHERE FLUID

In three dimensions, the Boltzmann-Enskog formula of the self-diffusion coefficient reads [63,64]

$$D_E = \frac{\pi^{1/2}\sigma}{16\eta g_2(\eta)}\left(\frac{k_B T}{m}\right)^{1/2}, \tag{B1}$$

where $g_2(\eta)$, the pair distribution function at contact, can be estimated using different expressions, e.g., the virial expansion, $g_{2,\text{virial}}(\eta) \simeq 1 + 2.5\eta + 4.5904\eta^2 + 7.36\eta^3$, or the simple, but accurate, Carnahan-Starling [65] expression, $g_{2,\text{CS}}(\eta) = \frac{1-\eta/2}{(1-\eta)^3}$.

The D_E expression extends the kinetic theory of (infinitely diluted) gases to finite packing fractions but neglects correlated motions between collisions since it relies on the molecular chaos approximation. As in two dimensions, a correction factor $h(\eta)$ can be introduced,

$$D_0 = D_E h(\eta), \tag{B2}$$

to account for these particular hydrodynamic effects (which can modify D_E by up to 40%). The two main correlation effects are the density and finite (domain) size.

The density effect is linked to a delayed back-scattering process which leads to an increase in the diffusion coefficient at intermediate packing fractions (due to extended vortex flows around a moving hard sphere) and a strong decrease at high packing fractions (due to caging effect). Since the pioneering work of Alder *et al.* [61], several empirical or semiempirical expressions have been devised for $h(\eta)$ (e.g., see [66–69] and [64] for a recent review).

The finite size of the computational domain or cell leads to a significant N dependence of D_0 when η is fixed. At intermediate packing fractions, hydrodynamic arguments lead to a correction in $N^{-1/3}$ for D_0, which has been confirmed by extensive MD simulations for a large set of finite periodic systems and various geometries [41,70–73]. At low and high packing fractions, however, a correction in N^{-1} has been conjectured [41], and a global, accurate fit over a wide range of packing fractions has been obtained,

$$D_0 = D_E h_0(\eta) - A(\eta)N^{-\alpha(\eta)}, \tag{B3}$$

where the expressions of $h_0(\eta)$, $A(\eta)$, and $\alpha(\eta)$ are explicitly given in Ref. [41].

As in two dimensions, it is hard to devise the finite-size correction for our system since it is not a finite periodic system. It is particularly difficult to estimate the relevant number of hard spheres to be used in Eq. (B3), the total number of hard spheres of the simulation clearly providing an upper limit only.

APPENDIX C: COMPOSITION OF THE STEADY-STATE SYSTEM

Let $\rho_1(r)$ and $\rho_0(r)$ denote the radial density of activated (blue) and deactivated (red) particles, respectively. Assuming that the Fokker-Planck equation with constant diffusivities can be applied, these densities evolve as

$$\frac{\partial\rho_k(r,t)}{\partial t} = \frac{1}{r^{d-1}}\frac{\partial}{\partial r}\left[Dr^{d-1}\frac{\partial\rho_k(r,t)}{\partial r}\right], \quad k = 0,1, \tag{C1}$$

in a d-dimensional system. The boundary conditions are

$$\rho_1(r_0,t) = \rho_0(r_1,t) = 0 \tag{C2}$$

and

$$\frac{\partial\rho_1(r_0,t)}{\partial t} = -\frac{\partial\rho_0(r_0,t)}{\partial t}, \quad \frac{\partial\rho_0(r_1,t)}{\partial t} = -\frac{\partial\rho_1(r_1,t)}{\partial t}. \tag{C3}$$

In the steady state for $d = 2$ we find

$$n_1(r) = c\ln(r/r_0), \quad n_0(r) = c\ln(r_1/r), \tag{C4}$$

where the constant c can be determined by calculating the total number of particles:

$$N = \int_{r_0}^{r_1}(\rho_1(r) + \rho_0(r))rdr = \frac{c}{2}\ln(r_1/r_0)\left(r_1^2 - r_0^2\right). \tag{C5}$$

Similarly, we find

$$N_1 = \frac{c}{4}\left(r_0^2 - r_1^2 + 2R_1^2\ln(r_1/r_0)\right) \tag{C6}$$

and the ratio is

$$\frac{N_1}{N} = \frac{\beta^2}{\beta^2 - 1} - \frac{1}{2\ln\beta}. \tag{C7}$$

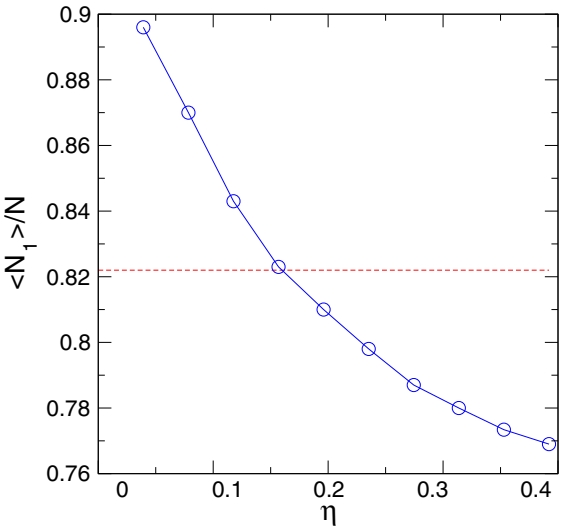

FIG. 16. Steady-state composition of the hard-disk system $R_0 = 0.5$, $R_1 = 8$ as a function of the packing fraction. The dashed line shows the value computed assuming that the diffusivities are uniform.

Figure 16 compares this formula with the composition found in the simulation. For low densities, the simulated composition exceeds the theoretical value. There is a crossover at $\eta \approx 0.15$ beyond which there are fewer active particles than predicted by a uniform diffusion model.

For $d \neq 2$ the equations are

$$\rho_1(r) = \frac{c}{2-d}\left(r^{2-d} - r_0^{2-d}\right), \quad \rho_0(r) = \frac{c}{2-d}\left(r_1^{2-d} - r^{2-d}\right) \tag{C8}$$

and

$$N = \frac{c}{d(2-d)}\left(r_1^d - r_0^d\right)\left(r_1^{2-d} - r_0^{2-d}\right), \tag{C9}$$

$$N_1 = \frac{c}{2-d}\left((1/d - 1/2)r_0^2 + (1/2)r_1^2 - (1/d)r_0^{2-d}r_1^d\right). \tag{C10}$$

For example, for $d = 3$ the fraction of active particles is

$$\frac{N_1}{N} = \frac{(1+2\beta)\beta}{2(\beta^2 - \beta + 1)}. \tag{C11}$$

APPENDIX D: INITIAL CONFIGURATION FOR EVENT-DRIVEN SIMULATIONS

Here we detail the procedure for generating the initial configuration. The hard-core particles are placed randomly and sequentially, without overlap in the annulus. This is an efficient method when $\eta < 0.45$ in two dimensions and $\eta < 0.25$ in three dimensions. To generate higher density systems either we start from an equilibrated large system with a low density and then gradually reduce the outer radius R_1 or we start from a regularly spaced, quasicrystalline configuration and let the system reach equilibrium. Random velocities, either uniformly, $-1 < v_{k,i} < 1, k = x, y$, or Gaussianly distributed, are assigned to a subsystem of $N - 1$ particles giving an angular momentum

$$\boldsymbol{L}_{N-1} = \sum_{i=1}^{N-1} \boldsymbol{r}_i \times m\boldsymbol{v}_i. \tag{D1}$$

The position vector of the last particle is selected so that it is perpendicular to $\boldsymbol{L}_{N-1}$ and its velocity, $\boldsymbol{v}_N$, is chosen so that the total angular momentum is 0:

$$\boldsymbol{L}_N = \boldsymbol{L}_{N-1} + \boldsymbol{r}_N \times m\boldsymbol{v}_N = \boldsymbol{0}. \tag{D2}$$

Finally, all the velocities are rescaled, $\boldsymbol{v}_i' = \alpha \boldsymbol{v}_i$, so that Eq. (3) is satisfied.

[1] H.-X. Zhou, G. Rivas, and A. P. Minton, Macromolecular crowding and confinement: Biochemical, biophysical, and potential physiological consequences, Annu. Rev. Biophys. **37**, 375 (2008).

[2] K. Aoki, K. Takahashi, K. Kaizu, and M. Matsuda, A quantitative model of erk map kinase phosphorylation in crowded media, Sci. Rep. **3**, 1541 (2013).

[3] M. Tabaka, T. Kalwarczyk, J. Szymanski, S. Hou, and R. Holyst, The effect of macromolecular crowding on mobility of biomolecules, association kinetics and gene expression in living cells, Front. Phys. **2**, 54 (2014).

[4] M. Currie, C. Thao, R. Timerman, R. Welty, B. Berry, E. D. Sheets, and A. A. Heikal, Multiscale diffusion of a molecular probe in a crowded environments: A concept, in *SPIE Optical Engineering + Applications* (International Society for Optics and Photonics, Bellingham, WA, 2015), p. 95840E.

[5] S. H. Schneider, S. P. Lockwood, D. I. Hargreaves, D. J. Slade, M. A. LoConte, B. E. Logan, E. E. McLaughlin, M. J. Conroy, and K. M. Slade, Slowed diffusion and excluded volume both contribute to the effects of macromolecular crowding on alcohol dehydrogenase steady-state kinetics, Biochemistry **54**, 5898 (2015).

[6] S. Hou, P. Trochimczyk, L. Sun, A. Wisniewska, T. Kalwarczyk, X. Zhang, B. Wielgus-Kutrowska, A. Bzowska, and R. Holyst, How can macromolecular crowding inhibit biological reactions? The enhanced formation of DNA nanoparticles, Sci. Rep. **6**, 22033 (2016).

[7] M. F. Shlesinger, Random searching, J. Phys. A Math. Theor. **42**, 434001 (2009).

[8] G. M. Viswanathan, S. V. Buldyrev, S. Havlin, M. Da Luz, E. Raposo, and H. E. Stanley, Optimizing the success of random searches, Nature **401**, 911 (1999).

[9] R. J. Ellis, Macromolecular crowding: Obvious but underappreciated, Trends Biochem. Sci. **26**, 597 (2001).

[10] A. P. Minton, The influence of macromolecular crowding and macromolecular confinement on biochemical reactions in physiological media, J. Biol. Chem. **276**, 10577 (2001).

[11] J. Dzubiella and J. McCammon, Substrate concentration dependence of the diffusion-controlled steady-state rate constant, J. Chem. Phys. **122**, 184902 (2005).

[12] J. S. Kim and A. Yethiraj, Effect of macromolecular crowding on reaction rates: A computational and theoretical study, Biophys. J. **96**, 1333 (2009).

[13] N. Dorsaz, C. De Michele, F. Piazza, P. De Los Rios, and G. Foffi, Diffusion-Limited Reactions in Crowded Environments, Phys. Rev. Lett. **105**, 120601 (2010).

[14] F. Piazza, N. Dorsaz, C. De Michele, P. De Los Rios, and G. Foffi, Diffusion-limited reactions in crowded environments: A local density approximation, J. Phys.: Condens. Matter **25**, 375104 (2013).

[15] J. D. Schmit, E. Kamber, and J. Kondev, Lattice Model of Diffusion-Limited Bimolecular Chemical Reactions in Confined Environments, Phys. Rev. Lett. **102**, 218302 (2009).

[16] J. N. Israelachvili, *Intermolecular and Surface Forces: Revised Third Edition* (Academic Press, New York, 2011).

[17] R. Evans, Fluids adsorbed in narrow pores: Phase equilibria and structure, J. Phys.: Condens. Matter **2**, 8989 (1990).

[18] T. Vanderlick, L. Scriven, and H. Davis, Molecular theories of confined fluids, J. Chem. Phys. **90**, 2422 (1989).

[19] M. M. Tomadakis and D. Rupani, Diffusion controlled reaction rate, survival probability, and molecular trajectory characteristics in the bulk, transition and Knudsen regime, Chem. Eng. J. **128**, 1 (2007).

[20] N. A. Licata, B. Mohari, C. Fuqua, and S. Setayeshgar, Diffusion of bacterial cells in porous media, Biophys. J. **110**, 247 (2016).

[21] J. Mittal, T. M. Truskett, J. R. Errington, and G. Hummer, Layering and Position-Dependent Diffusive Dynamics of Confined Fluids, Phys. Rev. Lett. **100**, 145901 (2008).

[22] S. Redner, *A Guide to First-Passage Processes* (Cambridge University Press, Cambridge, MA, 2001).

[23] O. Bénichou and R. Voituriez, From first-passage times of random walks in confinement to geometry-controlled kinetics, Phys. Rep. **539**, 225 (2014).

[24] C. Mejía-Monasterio, G. Oshanin, and G. Schehr, First passages for a search by a swarm of independent random searchers, J. Stat. Mech.: Theory Exp. (2011) P06022.

[25] P. Fauchald and T. Tveraa, Using first-passage time in the analysis of area-restricted search and habitat selection, Ecology **84**, 282 (2003).

[26] P. Turchin, Translating foraging movements in heterogeneous environments into the spatial distribution of foragers, Ecology **72**, 1253 (1991).

[27] B. Dybiec, E. Gudowska-Nowak, and P. Hänggi, Lévy-Brownian motion on finite intervals: Mean first passage time analysis, Phys. Rev. E **73**, 046104 (2006).

[28] J.-F. Rupprecht, O. Bénichou, and R. Voituriez, Optimal search strategies of run-and-tumble walks, arXiv:1603.03544.

[29] M. Knundsen, *The Kinetic Theory of Gases* (Methuen, London, 1950).

[30] E. Mason and A. Malinauskas, *Gas Transport in Porous Media: The Dusty-Gas Model. Chemical Engineering Monographs 17* (Elsevier, New York, 1983).

[31] R. Feres and G. Yablonsky, Knudsen's cosine law and random billiards, Chem. Eng. Sci. **59**, 1541 (2004).

[32] S. Miller, Insights into the second law of thermodynamics from anisotropic gas-surface interactions, Found. Phys. **37**, 1660 (2007).

[33] F. Celestini and F. Mortessagne, Cosine law at the atomic scale: Toward realistic simulations of Knudsen diffusion, Phys. Rev. E **77**, 021202 (2008).

[34] B. Alder and T. Wainwright, Phase transition in elastic disks, Phys. Rev. **127**, 359 (1962).

[35] C. Tejero and J. Cuesta, Hard-sphere and hard-disk freezing from the differential formulation of the generalized effective liquid approximation, Phys. Rev. E **47**, 490 (1993).

[36] F. Román, A. González, J. White, and S. Velasco, Velocity distributions for a hard-disk fluid in a small circular cavity: Effect of the conservation of the total angular momentum, Physica A **334**, 312 (2004).

[37] M. Uranagase, Effects of conservation of total angular momentum on two-hard-particle systems, Phys. Rev. E **76**, 061111 (2007).

[38] J. Haile, *Molecular Dynamics Simulation* (Wiley, New York, 1992).

[39] J. Carmer, F. van Swol, and T. M. Truskett, Note: Position-dependent and pair diffusivity profiles from steady-state solutions of color reaction-counterdiffusion problems, J. Chem. Phys. **141**, 046101 (2014).

[40] A. Szabo, K. Schulten, and Z. Schulten, First passage time approach to diffusion controlled reactions, J. Chem. Phys. **72**, 4350 (1980).

[41] D. M. Heyes, M. Cass, J. G. Powles, and W. Evans, Self-diffusion coefficient of the hard-sphere fluid: System size dependence and empirical correlations, J. Phys. Chem. B **111**, 1455 (2007).

[42] J. J. Erpenbeck and W. W. Wood, Molecular-dynamics calculations of the velocity-autocorrelation function. Methods, hard-disk results, Phys. Rev. A **26**, 1648 (1982).

[43] R. Garcia-Rojo, S. Luding, and J. J. Brey, Transport coefficients for dense hard-disk systems, Phys. Rev. E **74**, 061305 (2006).

[44] P. Hänggi, P. Talkner, and M. Borkovec, Reaction-rate theory: Fifty years after Kramers, Rev. Mod. Phys. **62**, 251 (1990).

[45] B. Liu, J. Goree, and O. Vaulina, Test of the Stokes-Einstein Relation in a Two-Dimensional Yukawa Liquid, Phys. Rev. Lett. **96**, 015005 (2006).

[46] R. Srivastava and K. Khanna, Stokes-Einstein relation in two- and three-dimensional fluids, J. Chem. Eng. Data **54**, 1452 (2009).

[47] R. Krishna and J. Wesselingh, The Maxwell-Stefan approach to mass transfer, Chem. Eng. Sci. **52**, 861 (1997).

[48] R. Krishna and J. M. van Baten, Investigating the validity of the Bosanquet formula for estimation of diffusivities in mesopores, Chem. Eng. Sci. **69**, 684 (2012).

[49] W. G. Pollard and R. D. Present, On gaseous self-diffusion in long capillary tubes, Phys. Rev. **73**, 762 (1948).

[50] J. Machta and R. Zwanzig, Diffusion in a Periodic Lorentz Gas, Phys. Rev. Lett. **50**, 1959 (1983).

[51] N. Chernov, Entropy, Lyapunov exponents, and mean free path for billiards, J. Stat. Phys. **88**, 1 (1997).

[52] P. Gaspard and J. Lutsko, Imploding shock wave in a fluid of hard-core particles, Phys. Rev. E **70**, 026306 (2004).

[53] N. A. Frej and D. C. Prieve, Hindered diffusion of a single sphere very near a wall in a nonuniform force field, J. Chem. Phys. **98**, 7552 (1993).

[54] H.-X. Zhou, Viewpoint: Speeding up in a crowd, Physics **3**, 77 (2010).

[55] S. Chandrasekhar, Stochastic problems in physics and astronomy, Rev. Mod. Phys. **15**, 1 (1943).

[56] A. Godec and R. Metzler, Optimization and universality of Brownian search in a basic model of quenched heterogeneous media, Phys. Rev. E **91**, 052134 (2015).

[57] G. Vaccario, C. Antoine, and J. Talbot, First-Passage Times in d-Dimensional Heterogeneous Media, Phys. Rev. Lett. **115**, 240601 (2015).

[58] F. Sedlmeier, Y. von Hansen, L. Mengyu, D. Horinek, and R. R. Netz, Water dynamics at interfaces and solutes: Disentangling free energy and diffusivity contributions, J. Stat. Phys. **145**, 240 (2011).

[59] G. Hummer, Position-dependent diffusion coefficients and free energies from Bayesian analysis of equilibrium and replica molecular dynamics simulations, New J. Phys. **7**, 34 (2005).

[60] K. E. Gubbins, Y.-C. Liu, J. D. Moore, and J. C. Palmer, The role of molecular modeling in confined systems: Impact and prospects, Phys. Chem. Chem. Phys. **13**, 58 (2011).

[61] B. J. Alder, D. M. Gass, and T. E. Wainwright, Studies in molecular dynamics. VIII. The transport coefficients for a hard-sphere fluid, J. Chem. Phys. **53**, 3813 (1970).

[62] M. Isobe, Long-time tail of the velocity autocorrelation function in a two-dimensional moderately dense hard-disk fluid, Phys. Rev. E **77**, 021201 (2008).

[63] J.-P. Hansen and I. R. McDonald, *Theory of Simple Liquids*, 3rd ed. (Academic Press, London, 2006).

[64] Á. Mulero, *Theory and Simulation of Hard-Sphere Fluids and Related Systems* (Springer, Berlin, 2008).

[65] N. F. Carnahan and K. E. Starling, Equation of state for non-attracting rigid spheres, J. Chem. Phys. **51**, 635 (1969).

[66] J. J. Erpenbeck and W. W. Wood, Self-diffusion coefficient for the hard-sphere fluid, Phys. Rev. A **43**, 4254 (1991).

[67] R. J. Speedy, Diffusion in the hard sphere fluid, Mol. Phys. **62**, 509 (1987).

[68] E. Ruckenstein and H. Liu, Self-diffusion in gases and liquids, Ind. Eng. Chem. Res. **36**, 3927 (1997).
[69] H. Sigurgeirsson and D. Heyes, Transport coefficients of hard sphere fluids, Mol. Phys. **101**, 469 (2003).
[70] B. Dünweg and K. Kremer, Molecular dynamics simulation of a polymer chain in solution, J. Chem. Phys. **99**, 6983 (1993).
[71] M. Fushiki, System size dependence of the diffusion coefficient in a simple liquid, Phys. Rev. E **68**, 021203 (2003).
[72] I.-C. Yeh and G. Hummer, System-size dependence of diffusion coefficients and viscosities from molecular dynamics simulations with periodic boundary conditions, J. Chem. Phys. B **108**, 15873 (2004).
[73] G. Kikugawa, T. Nakano, and T. Ohara, Hydrodynamic consideration of the finite size effect on the self-diffusion coefficient in a periodic rectangular parallelepiped system, J. Chem. Phys. **143**, 024507 (2015).